Chapter 3
Development of a finite element knee joint model

This chapter discusses the road taken to develop a finite element model of the knee joint. It starts with a study into different workflows to obtain meshed geometries and a study to investigate the amount of segmentation data necessary to obtain an adequate mesh. In the KneeHub project, team ABI developed multiple versions of the finite element knee joint models. The three different versions of the model are discussed with their advantages and limitations, and the final model development workflow is elaborated in more detail.

3.1 Comparison of five workflows to obtain bone and cartilage meshes for computational human knee modelling

This work was presented with a poster at the 11th Australasian Biomechanics Conference in Auckland, New Zealand, in 2018.

3.1.1 Introduction

Many decisions have to be made in model development, which makes the reproducibility of computational models questionable (Erdemir et al., 2019; Baker 2016). The first steps to build a computational knee joint model are segmentation and mesh generation. This study focused on the effect of different mesh generation workflows on the final geometry obtained. All methods used different amounts of segmentation data to reconstruct the geometries of the bones and cartilages of the knee joint. If less segmentation data would be necessary to obtain a mesh similar to a mesh obtained using segmentation data of the full imaging dataset, segmentation time and effort could be saved. This is a crucial step to overcome before finite element knee joint models could be widely used in the clinic.

3.1.2 Methods

Bone and cartilage meshes of 24 subjects were previously generated using an existing statistical shape model (SSM) (Zhang, Fernandez et al., 2016; Zhang, Hislop-Jambrich et al., 2016), and a previously established cartilage lofting workflow (Kazemi, 2018) as described in the KneeHub *model development phase* specifications documents available on: https://simtk.org/projects/kneehub. Principal component analysis (PCA) was performed on the bone meshes independently and on the bone and cartilage meshes combined. To train the linear regression and partial least squares

regression, one dependent variables training set, containing four bone and cartilage projected weights (PCs), explaining over 85% of the variance in the population, was used. Two separate independent variables training sets were used. The first training set included four bone only PCs, demographic and anthropometric data (gender, age, weight, height and body mass index (BMI)) and cartilage thickness data. The second training set included only the demographic and anthropometric data and the cartilage thickness data.

Five different mesh generation workflows were compared by reconstructing the bone and cartilage meshes from predicted PC weights of a subject inside the training set of the statistical shape models (Figure 3.1). The obtained meshes were compared by calculating the mean distance between the obtained mesh and the initially segmented point cloud. In the first workflow (pink), the mesh was directly obtained using a previously established statistical shape model and cartilage lofting. Two workflows used the linear regression (LR) model, where one used training set 1 (black, $R^2 = 1.00$), and the other used training set 2 (orange, $R^2 = 1.00$). The remaining two workflows used partial least squares regression (PLSR), one using training set 1 (green, $R^2 = 0.99$) and the other using training set 2 (blue, $R^2 = 0.87$).

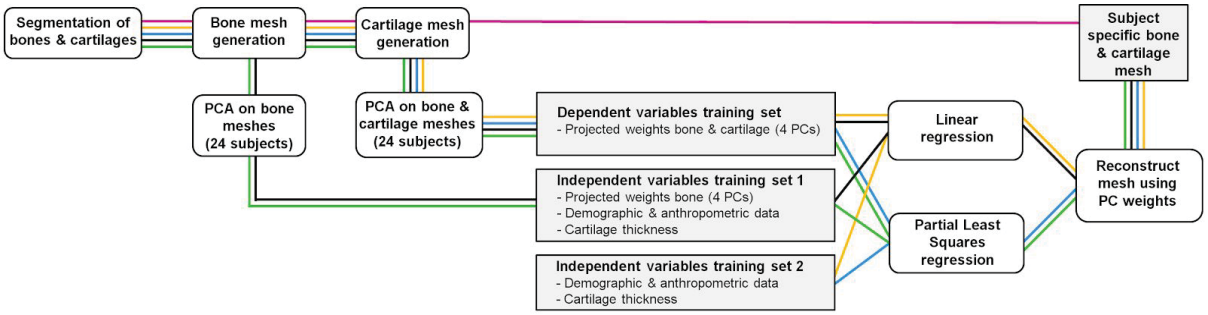

Figure 3.1: Five workflows to obtain bone and cartilage meshes of the knee, Pink: obtaining the mesh using a previously established SSM and cartilage lofting, Black: LR using training set 1 (mean $R^2 = 1.00$), Orange: LR using training set 2 (mean $R^2 = 1.00$), Green: PLSR using training set 1 (mean $R^2 = 0.99$), Blue: PLSR using training set 2 (mean $R^2 = 0.87$).

3.1.3 Results

The mean distances of the obtained meshes using the five different workflows to the initially segmented point clouds are presented in Figure 3.2. No marked differences were found between the meshes obtained using the various workflows, except for the femur obtained with the PLSR workflow that used training set 2, which showed a larger mean distance.

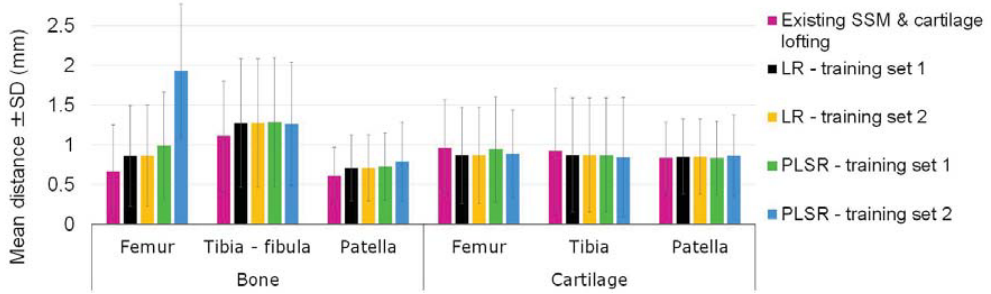

Figure 3.2: Mean distances between the obtained bone and cartilage meshes and the segmented 3D point clouds for all five workflows.

3.1.4 Discussion & conclusion

The five workflows provided meshes with a similar distance to the original segmentations, except for the femur bone mesh obtained using PLSR and training set 2. This suggests that for most workflows, the choice of workflow did not affect the obtained geometry. We hypothesise that this is partly due to predicting the geometry of a subject included in the training sets of the LR and PLSR models. It remains to be seen whether the subtle changes in geometry will result in differences in joint mechanics following a simulation.

The content of the independent variables training sets is questionable. Per subject, there were only four data points for PCs, five data points for the demographic and anthropometric data, and 5950, 2612 and 1089 for the femur, tibia and patella cartilage thickness values, respectively. This would mean that the LR and PLSR would not be very sensitive to changes in the PC weights and the demographic and anthropometric data. We would prefer to only use the PC weights and demographic and anthropometric data to predict bone and cartilage meshes since this would decrease data collection time and effort. Repeating the study by using different independent variables training sets should be considered.

With the LR R^2 values of 1.00 and by predicting the bone and cartilage PC weights of a subject inside the training set, the distances between the reconstructed meshes and the segmentations arise from the reconstruction using only four PCs with 85% of the variability in the population explained. In future work, the training set should be increased with a representative sample population, and the ability of these workflows to predict the geometry of a subject outside of the training set should be investigated.

3.2 The influence of segmentation on mesh generation

This work was presented on a poster at the 11th Australasian Biomechanics Conference in Auckland, New Zealand, in 2018.

3.2.1 Introduction

Image segmentation is a time-consuming step in computational knee joint modelling and is prone to human error. Therefore, methods to decrease this time and potentially automate the process should be investigated before the potential use of subject-specific models in the clinic. This study investigated the intra- and inter-rater segmentation accuracy and the influence of segmented point cloud data sparseness on the final meshed geometries. If similar meshes could be obtained by segmenting only parts of the imaging data in comparison to meshes obtained using segmentations of the entire imaging data set, segmentation time could be decreased considerably. This would increase the potential of using subject-specific computational models in the clinic.

3.2.2 Methods

3.2.2.1 Intra- and inter-rater segmentation accuracy

One set of 112 slices of general-purpose sagittal MRI data (Natural Knee Data, Denver University (Harris et al., 2016; Ali et al., 2016; https://digitalcommons.du.edu/natural_knee_data/), was segmented using a custom MATLAB script, obtaining 3D point clouds (Figure 3.3). The intra- and inter-rater accuracy was calculated by comparing the mean cloud to cloud distances of the segmented 3D point clouds. For this study, the bones and cartilages of the knee joint (femur, tibia and patella) were segmented three times by the same and one time by another researcher (three times intra- and one time inter-rater).

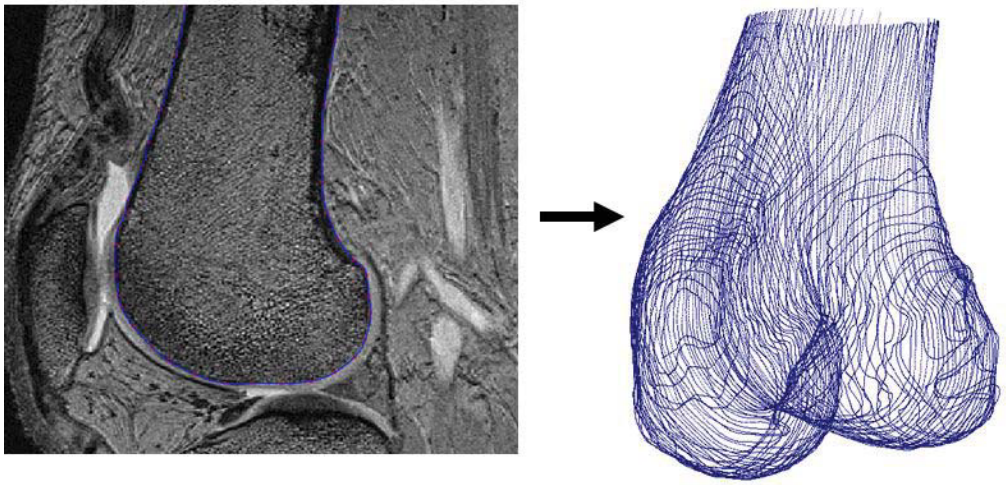

Figure 3.3: Left: Segmented MRI data, using a custom MATLAB script, Right: Segmented 3D point cloud of the distal femur.

3.2.2.2 Sparseness of segmentation data

The sparseness of the bone segmentation data was decreased using three different methods. In the density reduction (DR) method, random sampling using CloudCompare software (CloudCompare version 2.10-alpha) was used to reduce the number of data points to 5, 10, 25, 50 and 75% of the whole segmentation. In the slice reduction (SR) method, only the segmentations of 5, 9 and 17 slices of the MRI were used to obtain the meshes. In the human informed method (HI), during segmentation, only the points which seemed to be significant to the segmenter were selected, with no restriction to which slices had to be segmented and no further directions given. This was executed three times. For all density reduced segmentation data and the full segmentation data, the corresponding bone meshes were obtained using a pre-established workflow using a SSM and cartilage lofting (Kazemi, 2018) as described in the KneeHub *model development phase* specifications documents available on *https://simtk.org/projects/kneehub*. The distances between the obtained meshes and the full segmentation data were obtained using the cloud to cloud distance tool in the CloudCompare software.

3.2.3 Results

3.2.3.1 Intra- and inter-rater segmentation accuracy

The intra- and inter-rater cloud to cloud distances of the segmentations are shown in Table 3.1. The inter-rater distances were larger than the intra-rater distances.

Table 3.1: Mean femur, tibia and patella bone and cartilage segmentation distances.

	Bone (mm) (±SD)	Cartilage (mm) (±SD)
Intra-rater (n=3)	0.363 ± 0.025	0.308 ± 0.079
Inter-rater (n=1)	0.457 ± 0.060	0.592 ± 0.320

3.2.3.2 Sparseness of segmentation data

The cloud to cloud distances between the full segmentation and the meshes obtained using DR, SR, HI, and full segmentation can be found in Figure 3.4. With increasing segmentation point cloud density (DR method), the distance decreased for the femur. However, this was not the case for the other bones, where no stable trend of increasing density with decreasing distance was found. With an increasing number of slices used in the SR method, the distances decreased for all bones. The slice reduction method using 17 slices showed similar results compared to using the full segmentation to obtain the mesh. The distances of the meshes using the HI method were slightly larger than the distances found with the mesh obtained using the full segmentation.

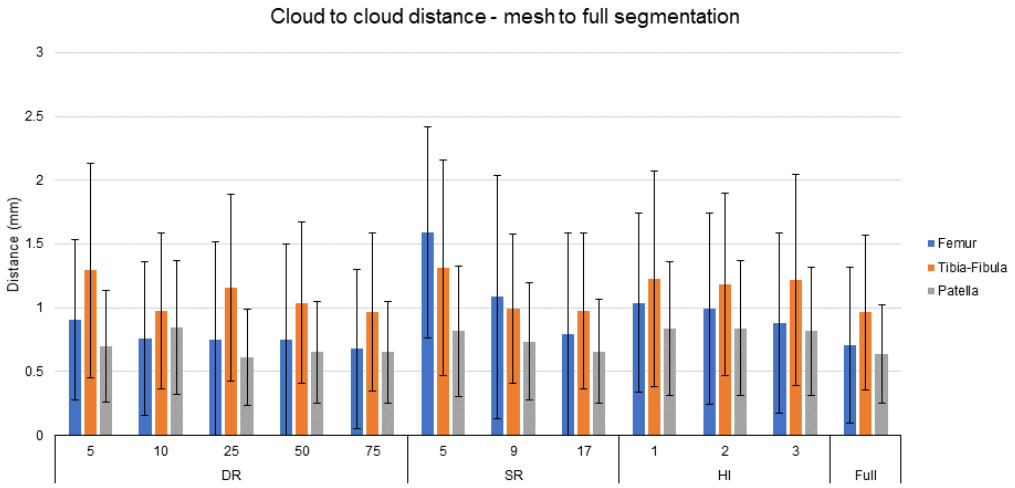

Figure 3.4: Cloud to cloud distances ±SD of the obtained meshes to the full segmentation for the meshes obtained using density reduction (DR), slice reduction (SR), the human informed (HI) and the full segmentations.

3.2.4 Discussion & conclusion

3.2.4.1 Intra- and inter-rater segmentation accuracy

The inter-rater distances were larger than the intra-rater distances, which emphasises the human factor in segmentation. An automatic SSM based segmentation tool might be used to reduce this factor. Considering the cartilage only being a few millimetres thick, the cloud to cloud distances for the cartilages were high.

3.2.4.2 Sparseness of segmentation data

Results showed similar distances to the full segmentation of the mesh obtained with 17 slices of MRI data and the mesh obtained using the full segmented MRI data set (112 slices). If this effect is still seen after increasing the number of MRI data sets in this study, this might indicate that the same results could be obtained using less segmentation data, which would decrease segmentation times significantly. The distances to the full segmentation of the meshes using the HI method were found to be slightly larger than the distances found with the mesh obtained using the full segmentation. This difference might not be large enough to cause significant differences in the kinematic outcomes of the models, but by using this method, the segmentation time could be decreased significantly (~6x shorter). In future work, computational models could be built from the meshes obtained using the 17 slices MRI and the HI segmentations to study the influence of segmentation sparseness on kinematic predictions.

In the DR method, the selected points might have influenced the weights of the fitted PCs to the point cloud. This might imply that the mesh obtained was dependent on which points were randomly selected. For this reason, the results of this method were not analysed.

3.3 Development of finite element knee joint models

3.3.1 Introduction

In the KneeHub project, five teams were given the same two imaging and cadaveric laxity datasets to develop a tibiofemoral joint model simulating 0 to 90 degrees of knee flexion, investigating the “art” of computational knee joint modelling. The models in this chapter were developed during the *model development* and *model calibration phase* of the KneeHub project. This chapter discusses three versions of the models, giving insight into the decisions made during model development and providing details on the final model development workflow established. The model development methods of the three model versions are summarised. The complete methods can be found in the deliverables of the *model development* and *model calibration* phase of the KneeHub project, available on: https://simtk.org/projects/kneehub.

3.3.2 Methods

3.3.2.1 Datasets provided

Two sets of cadaveric imaging and joint laxity data were provided in the KneeHub project. The teams were free to decide which parts of the data to use. The demographic and anthropometric data of the subjects are summarised in Table 3.2.

The first dataset, du02, is part of the Natural Knee dataset (Harris et al., 2016; Ali et al., 2016; https://digitalcommons.du.edu/natural_knee_data/). In this dataset, the following data was provided at the start of the *model development phase*:

- Magnetic resonance imaging (MRI) (sagittal and fat-suppressed)
- Clinical computed tomography (CT)
- Digitized probed points on the femur, tibia, and patella

Specimen-specific laxity data obtained using a robotic rig was added at the start of the *model calibration phase*.

The second dataset, oks003, is part of the Open Knee(s) dataset (Bennetts et al., 2015; Bonner et al., 2015; Colbrunn et al., 2015; Erdemir et al., 2015; https://simtk.org/projects/openknee). The following data was provided at the start of the *model development phase*:

- general-purpose MRI (3D T1-weighted without fat suppression - isotropic voxel size)
- cartilage imaging MRI (3D T1-weighted with fat suppression - anisotropic voxel size)
- soft tissue imaging (proton-density, turbospin echo) - axial plane MRI
- soft tissue imaging - sagittal plane MRI
- soft tissue imaging - coronal plane MRI

The following data was added at the start of the *model calibration phase*:

- Digitized probed points on the femur, tibia, and patella
- Specimen-specific laxity data obtained using a robotic rig

Table 3.2: Demographic and anthropometric characteristics of the datasets provided.

	du02	**oks003**
Age (years)	44	25
Sex	Male	Female
Height (m)	1.83	1.73
Mass (kg)	70.31	68
Right or left knee	Right	Left

3.3.2.2 Model version 1

Model version 1 was developed during the KneeHub model development phase. More detail on model version 1 can be found in the ABI KneeHub Model Development Phase Specifications documents available on: https://simtk.org/projects/kneehub.

The initial finite element model was developed only with the du02 specimen data using a workflow based on a previously established workflow (Kazemi, 2018). An overview is presented in Figure 3.5.

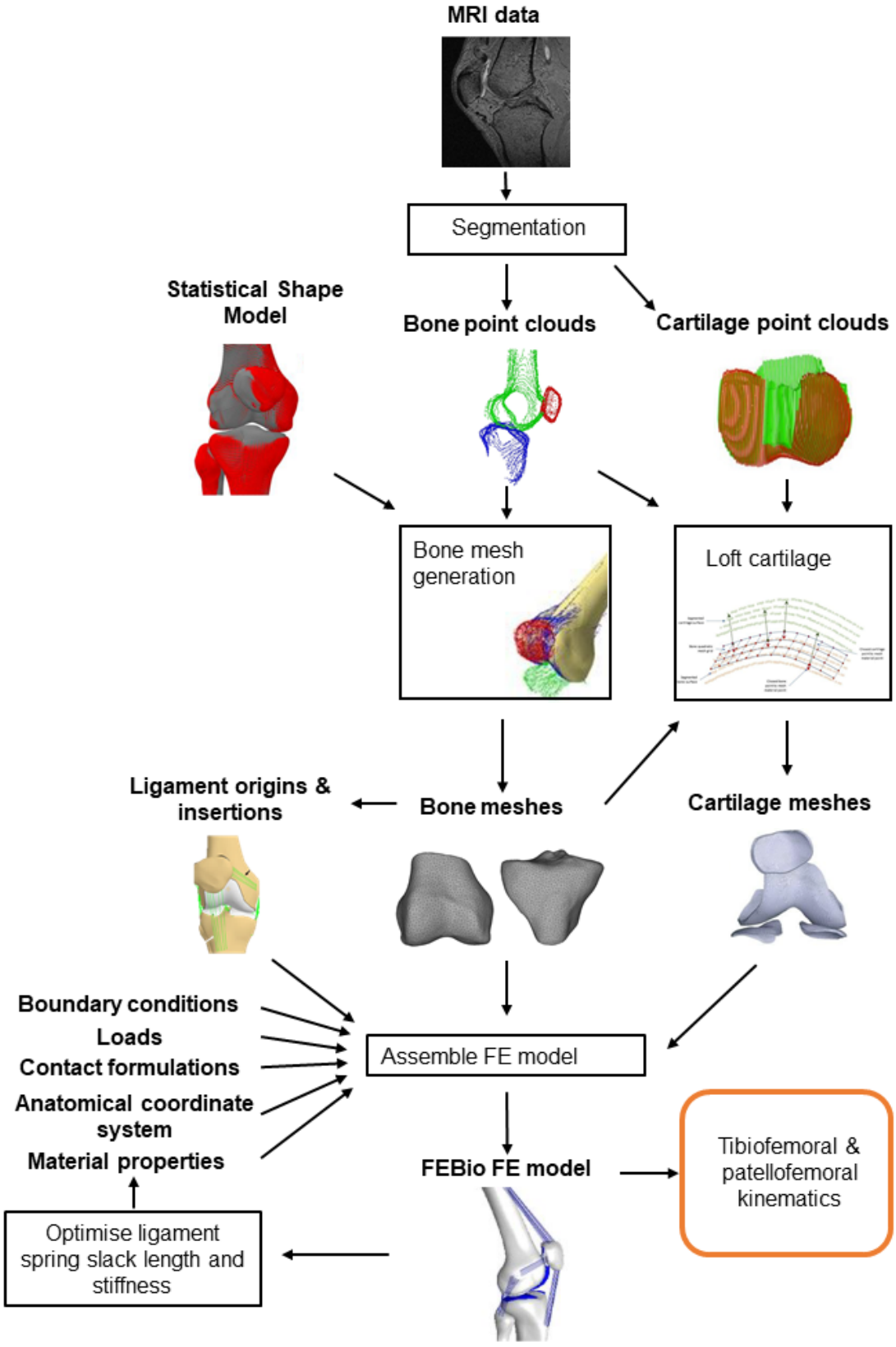

Figure 3.5: Overview of model development workflow version 1.

3.3.2.2.1 Segmentation & bone and cartilage mesh generation

The general purpose sagittal plane MRI imaging data of specimen du02 were manually segmented using a custom MATLAB script to obtain the point clouds of the distal femur, proximal tibia, proximal fibula and patella bones and the femoral, tibial and patellar cartilages. The bone meshes were generated using a SSM (Zhang, Fernandez et al., 2016; Zhang, Hislop-Jambrich et al., 2016). For this, the Musculoskeletal Atlas Project (MAP) client (Zhang et al., 2014) was used to perform rigid registration, principal component fitting and local fitting to the segmented bone point clouds to obtain triangulated .stl meshes of the bones. The three-layered hexahedral cartilage meshes were obtained by cartilage “lofting” from the bone mesh to the segmented cartilage point cloud using custom Python code (Kazemi, 2018).

3.3.2.2.2 Ligament & menisci representation

The tibiofemoral and patellofemoral ligament, tendon and joint capsule structures included (Table 3.3) were modelled as multiple uniaxial non-linear tension only spring elements. The menisci were modelled using three linear springs for each meniscus (2x anterior-posterior direction and 1x medial-lateral direction) (Li et al., 1999). The origins and insertions of the springs were extracted from the SSM.

Table 3.3: Ligament, tendon and joint capsule structures included in model version 1.

Tibiofemoral joint	**Patellofemoral joint**
Anterior cruciate ligament (ACL)	Patellar tendon (PT)
Posterior cruciate ligament (PCL)	Lateral patellofemoral ligament (LPFL)
Lateral collateral ligament (LCL)	Medial patellofemoral ligament (MPFL)
Medial collateral ligament (MCL)	Quadriceps tendon (QT) (Force vectors)
Popliteofibular ligament (PFL)	
Oblique popliteal ligament (OPL)	
Medial posterior capsule (MPC)	
Lateral posterior capsule (LPC)	

3.3.2.2.3 Constitutive models

The bones and cartilages were modelled as rigid bodies. The initial ligament and meniscus spring properties were based on literature.

3.3.2.2.4 Model assembly

The bone and cartilage meshes were assembled into a finite element model to be solved using FEBio software (Maas et al., 2012). Model version 1 was assembled with the knee joint in full extension.

3.3.2.2.4.1 Loads & boundary conditions

The femur was fixed in all six degrees of freedom (DOF), whereas the tibia was only fixed in the flexion-extension rotation DOF. The fibula was rigidly tied to the tibia. The patella was free in all six DOF, and a constant quadriceps force was applied to the patella for stabilisation.

3.3.2.2.4.2 Contact formulations

The bones and their corresponding cartilages were rigidly tied. Frictionless facet-on-facet sliding was applied to the cartilage-cartilage contact areas.

3.3.2.2.4.3 Anatomical coordinate system

To calculate the kinematics of the tibiofemoral and patellofemoral joint, the anatomical coordinate system described by Grood and Suntay was implemented (Grood & Suntay, 1983) using anatomical landmarks embedded in the SSM.

3.3.2.2.5 Ligament optimisation

The ligaments were initially optimised with the knee in full extension to laxity curves obtained from the literature (Li et al., 2002; Roth et al., 2015). All the springs of one ligament were optimised to one value for the stiffness and reference strain. Custom Python code was used to compare the literature load-displacement properties of the knee with those in the model by performing load-driven AP, IE and VV simulations. The reference strain and stiffness of the springs were optimised using a truncated Newton optimisation algorithm.

3.3.2.3 Model version 2

Model version 2 was submitted at the end of the model development phase of the KneeHub project. More detail on model Version 2 can be found in the ABI KneeHub Model Development Phase Deviations documents available on: https://simtk.org/projects/kneehub.

To address the limitations of model version 1, adjustments were made, which are described below, resulting in model version 2. A version 2 model was obtained for both datasets du02 and oks003. An overview of the model development workflow version 2 is presented in Figure 3.6.

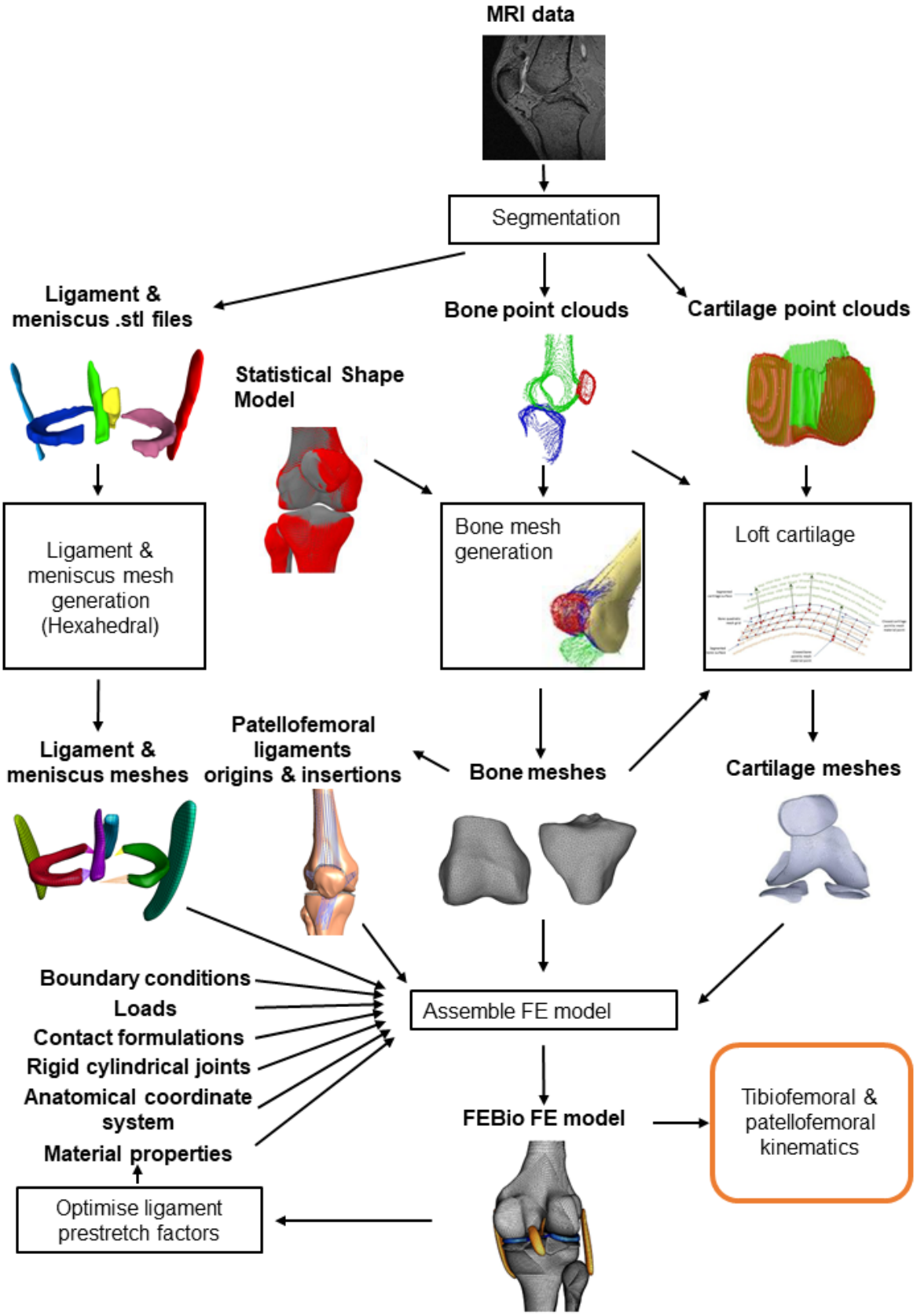

Figure 3.6: Overview of model development workflow version 2.

3.3.2.3.1 Bone & cartilage mesh generation

The bone & cartilage meshes were generated as in model version 1. The mesh development workflow, SSM fitting a Lagrangian mesh to the bones and lofting the cartilage was only functional for right knee joint data. However, the oks003 dataset is of a left knee. To accommodate for this, the oks003 segmentation data was mirrored to resemble a right knee, resulting in a right knee model for both datasets.

3.3.2.3.2 Ligament & meniscus representation

Compared to model version 1, the four main ligaments, including the ACL, PCL, MCL, and LCL, were modelled as continuum meshed geometries in model version 2, and the other ligaments were removed. The du02 MRI data were used to build template ligament meshes existing of hexahedral elements. These meshes were also used in the oks003 model. The template ligament meshes were obtained by segmenting the ligaments from the MRI data in Stradwin (Stradwin 5.4, Cambridge University Engineering Department, United Kingdom), smoothing the data in MeshLab (MeshLab, Istituto di Scienza e Tecnologie dell'Informazione, Pisa, Italy) and obtaining hexahedral meshes using IA-FEMesh (IA-FEMesh1.0, University of Iowa, USA). The resulting meshes were imported in Preview (Preview version 2.1.0, Musculoskeletal Research Laboratories, University of Utah, USA), where a final refinement and smoothing of the hexahedral meshes was performed.

The ligaments were manually put into the model as close as possible to the anatomical location. A simulation was performed, enabling a tied contact between the ends of the ligaments to their attachment locations on the bones, with the bones and cartilages fully constrained. The resulting ligament node coordinates were used as initial ligament node coordinates.

Since the three linear spring menisci model (Li et al., 1999) did not give the desired results in model Version 1, the menisci were modelled as deformable continuum geometries. We used the du02 MRI data to build template meshed geometries of the menisci, which were also used in the oks003 model. The template menisci meshes were created by segmenting the menisci from the MRI data in Stradwin (Stradwin 5.4, Cambridge University Engineering Department, United Kingdom), smoothing the data in MeshLab (MeshLab, Istituto di Scienza e Tecnologie dell'Informazione, Pisa, Italy) and obtaining hexahedral meshes using IA-FEMesh (IA-FEMesh1.0, University of Iowa, USA). The resulting meshes were imported in Preview (Preview version 2.1.0, Musculoskeletal Research Laboratories, University of Utah, USA), where a final refinement and smoothing of the hexahedral meshes was executed.

To increase model stability, the number of springs in the patellofemoral model was increased to disperse the force. The number of springs in the patellar tendon was increased from 5 to 18, and the number in the lateral and medial patellofemoral ligament was increased from 5 to 7 springs each. Next to that, 18 springs (0.5N per spring) instead of nodal loads were used for the quadriceps tendon force to ensure the line of action remained in the right direction since the femur was no longer fixed in all DOF.

3.3.2.3.3 Constitutive models

The bones and cartilages were modelled as rigid bodies as in model version 1. The uncalibrated material properties of the ligaments were prestrained transversely isotropic Mooney-Rivlin as in the MCL of the Open Knee (Erdemir & Sibole, 2010). The menisci material properties were based on the Open Knee (Erdemir & Sibole, 2010), with each horn attachment to the tibia represented by 35 linear springs with a stiffness of 20 N/mm per spring.

3.3.2.3.4 Model assembly

Model version 2 was assembled with the knee in full extension.

3.3.2.3.4.1 Loads & boundary conditions

To increase model stability, the tibia was fixed in 6 DOF, and the femur was free in 5 DOF with one DOF prescribed (flexion-extension). An axial force of 50 N was added in the du02 model to ensure cartilage-cartilage contact.

3.3.2.3.4.2 Contact formulations

To further increase model stability, the contact formulations were changed into sliding-elastic contact formulations since these were designed for areas with high compression forces according to the FEBio manual (Maas et al., 2012). A frictionless sliding elastic contact was also used between the menisci and the tibiofemoral cartilages.

Changing the representation of the ligaments required additional contact definitions between the bones and ligaments. A rigid tied contact was defined between the ligaments and their bony origins and insertions. A frictionless facet-on-facet sliding contact was formulated between the MCL and the tibia and femur bones and cartilages to avoid penetration.

3.3.2.3.4.3 Rigid cylindrical joints

In FEBio, it is not possible to mix free and prescribed DOF using rigid bodies directly. Therefore, three rigid cylindrical joints, using two dummy rigid bodies as specified in the Open Knee(s) models (Erdemir & Sibole, 2010), were added to the model to be able to mix prescribed and free rigid body rotations. This was necessary since we prescribed the knee flexion angle, where the other DOF of the knee joint were free.

3.3.2.3.5 Ligament optimisation

To accommodate for the continuum tibiofemoral ligaments, the ligament prestretch factor was optimised instead of the slack length and stiffness of the springs. The ligaments of model Version 2 were only optimised for anterior-posterior drawer and internal-external rotation at 0 degrees of knee flexion. The same calibration laxity data from the literature as in model version 1 was used (Li et al., 2002). The prestretch factors of the four main ligaments were optimised by applying a displacement and minimising the difference in model and literature load for each converged step. A calibration at 0

and 90 degrees of knee flexion was intended but was not successful since the FEBio restart feature was not working at the time. The FEBio restart feature is necessary to decrease optimisation time by not having to simulate 0 to 90 degrees in each iteration of the objective function.

3.3.2.3 Model version 3

Model version 3 was submitted at the end of the model calibration phase. More detail on model version 3 and the model files can be found in the ABI KneeHub Model Calibration Phase Deviations documents and M&S outputs folder available on: https://simtk.org/projects/kneehub.

New models were built using new meshed geometries to reduce the convergence issues we were experiencing in model version 2. The patellofemoral joint was excluded from the model to decrease the complexity of the model and increase convergence. The du02 dataset was modelled as a right and the oks003 dataset as a left knee. Subject-specific ligaments and menisci, which stayed in their imaging state, were used to ensure their location in the knee joint and their morphology at the start of the simulations. For all geometries, except for the bones, tetrahedral elements were used instead of hexahedral elements since these were easier to obtain, and the quality of the meshes could be checked in FEBio Preview software (Preview version 2.1.0, Musculoskeletal Research Laboratories, University of Utah, USA). An overview of the model development workflow version 3 is presented in Figure 3.7.

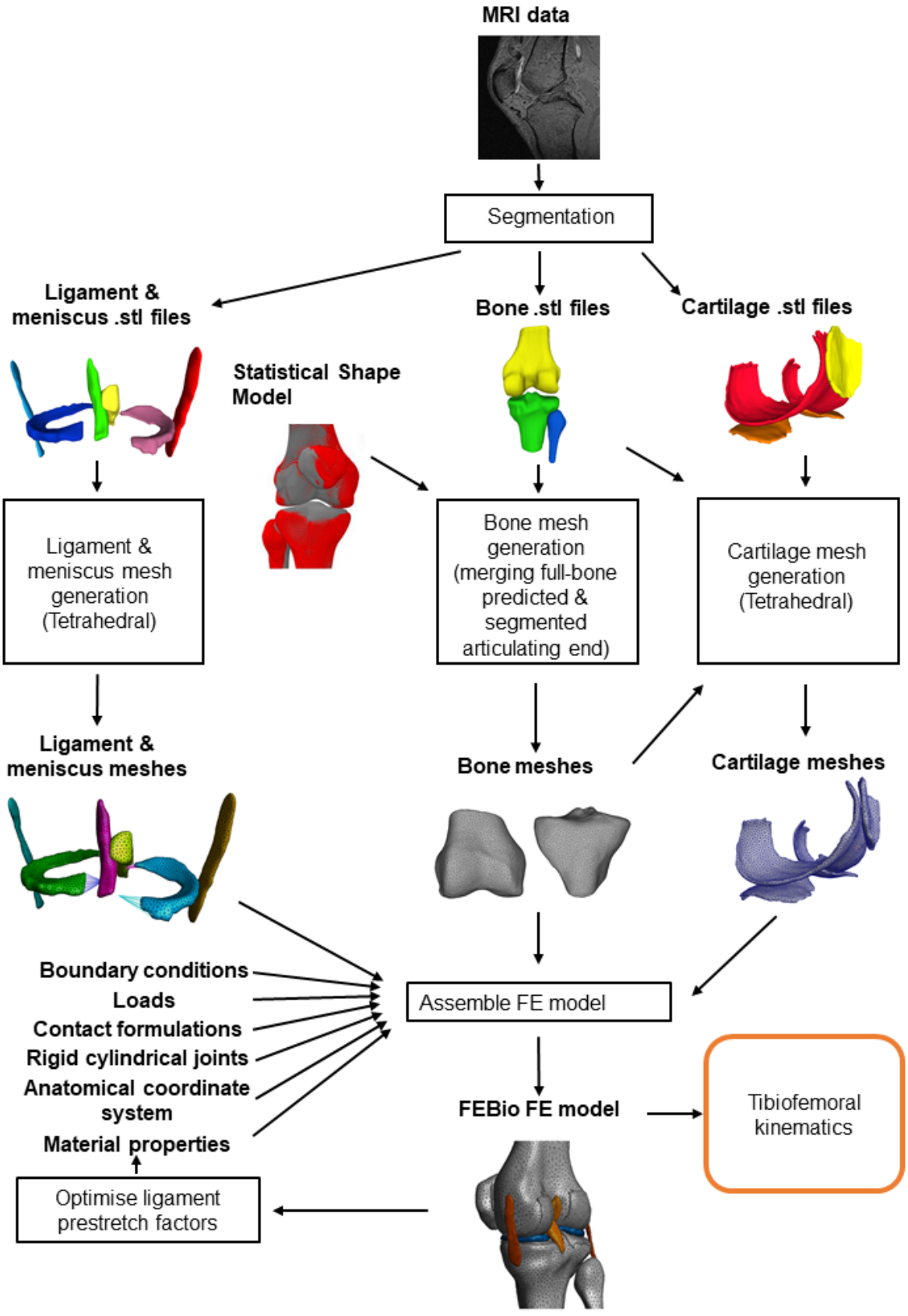

Figure 3.7: Overview of model development workflow version 3.

3.3.2.3.1 Segmentations

The imaging data were segmented again using Stradview (Version 6.0, Cambridge University Engineering Department, United Kingdom) for the du02 dataset & ITK-Snap (Version 3.6.0, Apr. 1 2017) for the oks003 dataset to generate .stl mesh files. These .stl files were needed to merge the segmented bone meshes with the SSM mesh as described in Section 3.3.2.3.2.1.

3.3.2.3.2 Mesh generation

3.3.2.3.2.1 Bone mesh generation

The femur and tibia-fibula bone segmentations were cut off to have open ends and saved as .ply files in CloudCompare (version 2.10-alpha, https://www.danielgm.net/cc/). In MeshLab (version 2016.12 https://www.meshlab.net/), the femur and tibia-fibula bone segmentations were Poisson-disk sampled to obtain point clouds. To get a good SSM fit (with the correct bone length), the probed femur hip ball points were used next to the distal femur segmentation point cloud to fit the SSM in MAPClient (Zhang et al., 2014). The femur hip ball points were aligned to the segmentation using robot probed points of the distal femur using CloudCompare. This resulted in a combined segmentation point cloud and hip ball probed points point cloud, which was used as input in MAPClient for the SSM fit of the femur.

Using MAPClient, seven principal components were used to fit the SSM to the femur segmentation and hip ball points, resulting in a fitting RMS of 2.048 mm. For the tibia-fibula bones, a SSM fit on the segmentation using ten principal components resulted in the lowest RMS fitting error (1.055 mm). The resulting .geof files were transformed into a .ply file using a custom Python script.

We strived to ensure that the articulating region resembled the segmented knee joint as close as possible. We merged the SSM-predicted full-length bones with the segmentation .ply files of the articulating ends of the femur, tibia and fibula. This was done in CloudCompare, where the whole bone mesh was aligned to the segmentation, and the full bone mesh generated in MAPClient was cut off where it overlapped with the segmentation. The cut-off full bone mesh and the segmentation were then merged into one mesh and loaded into MeshLab. At this point, the tibia and fibula were split into two geometries. All three bones were resampled using Poisson-Disk sampling (Femur 22000, Tibia 15000 and Fibula 14600 points). A Screened Poisson Surface Reconstruction was performed, and if needed, parts of the meshes were deleted, and the holes were closed before resampling and reconstructing the mesh again. When importing the meshes into Preview, it was found that the meshes were very dense, slowing down the simulations. Therefore they were simplified using the Quadric Edge Collapse Decimation function in MeshLab (Number of faces: Femur = 15,000, Tibia = 10,000, Fibula = 5,000 and Patella = 2,500), before importing them into Preview again.

3.3.2.3.2.2 Cartilage, ligament & meniscus mesh generation

The segmentation files of the cartilages, ligaments and menisci were saved as .ply files in MeshLab to facilitate import into FEBio Preview software (Preview version 2.1.0, Musculoskeletal Research

Laboratories, University of Utah, USA). If irregularities were present on the segmentations, these parts were removed, holes were closed, and the segmentation was smoothed (Laplacian) in MeshLab. These segmentations were then resampled to 4,000 points, the normals were computed, and a Screened Poisson Surface Reconstruction was performed, resulting in .stl files.

The cartilage .stl files from MeshLab were loaded into Preview for Tetrahedral mesh generation. The tibia cartilage was split into medial and lateral tibial cartilage. The segmentation .ply files were decimated (0.05), smoothed (preserving boundary and shape), and tetrahedral elements were generated with a radius edge ratio of 1 in Preview. The mesh was saved as a .ele file.

The ligament and menisci .stl files from MeshLab were imported in Preview. They were decimated, and TetGen was applied, changing the decimation factor (0.05 – 0.2) and the minimum edge ratio (1-3) in TetGen to obtain the best Tet Quality. If the Tet Quality was as low as possible (optimal = 0.62), the mesh was saved as a .ele file.

3.3.2.3.3 Constitutive models

The ligament material model was changed from transversely isotropic Mooney-Rivlin into a Neo-Hookean material model to enable intuitive adjustment of the ligament material properties. We investigated the influence of the ligament Young's modulus and prestretch factor values on model outcomes using basic sensitivity studies (available on: *https://simtk.org/projects/abi_knee_models*). The literature values for Young's modulus and Poisson's ratio (Table 3.4) (Orozco et al., 2018) were found to be sufficient. In the sensitivity studies, the ligament prestretch factor value bounds were found to be used in model calibration, where all ligaments' prestretch factor values were optimised individually (Chapter 6). The menisci kept the same material model as in model Version 2.

Table 3.4: Ligament material model Young's modulus and Poisson's ratio used in model version 3. The values were adapted from Orozco et al. (Orozo et al., 2018).

	ACL	PCL	MCL	LCL
Young's modulus (MPa)	123	168	224	280
Poisson's ratio	0.4	0.4	0.4	0.4

3.3.2.3.4 Model assembly

Model version 3 was not assembled in full extension but maintained in the imaging state as segmented. This ensured that all knee structures were in their correct position and orientation. The influence of a changing number of nodes in the tied contact for the ACL was investigated (*https://simtk.org/projects/abi_knee_models*). Differences in the simulated kinematics were found, but they were considered insignificant. It was decided to include the ligament nodes in overlap with the bone mesh to be included in the rigid tied contact. The menisci were connected to the tibia by springs. In model version 2, these springs had a stiffness of 20 N/mm. This was changed into 1 N/mm since this seemed to be stiff enough to keep the menisci in place.

3.3.2.3.4.1 Rigid cylindrical joint

In model version 3, the axes and origins of the Grood & Suntay ACS were set in the RCJs. This made it easier to apply the loads and prescribe or restrict displacements or rotations in the Grood & Suntay ACS description. The settings of the parameters of the RCJs were adapted from the Open Knee(s) models (*https://simtk.org/projects/openknee*).

3.3.2.3.4.2 Contact formulations

A rigid tied contact between the ligaments and the bones was used. In model version 3, we used nodes instead of surfaces in the rigid tied contact, improving the contact formulation. All contact formulations, except for the rigid tied contacts of the ligaments, were set to sliding-elastic. No facet-on-facet sliding contact between the MCL and the femur and tibia was used since this did not significantly influence the model simulation outputs, and removing this contact reduced convergence time. Sensitivity studies were performed on a couple of contact parameters. The methods and results of these sensitivity analyses on model parameters can be found on *https://simtk.org/projects/abi_knee_models*.

3.3.2.3.4.3 Loads & boundary conditions

Compared to version 2 of the models, no axial load to ensure cartilage-cartilage contact was applied to the femur in version 3 of model du02.

3.3.2.3.4.4 Control settings

To improve convergence and decrease computational time, sensitivity studies were performed on the control settings, looking at model convergence, computational time and model kinematics. The methods and results of the sensitivity studies on model parameters can be found on *https://simtk.org/projects/abi_knee_models*.

3.3.2.3.5 Finite element solver software

For model version 3, we used FEBio 3.0.0 since the previously used version 2.9.0 showed bugs regarding the restart function.

3.3.3 Results

3.3.3.1 Model version 1

Version 1 of the model was able to simulate 0 to 114 degrees of passive knee flexion by applying a rigid body moment to the tibia. The knee joint model at 0 and ~90 degrees of knee flexion is shown in Figures 3.8 and 3.9. In ~90 degrees of knee flexion, the femur was located far posteriorly compared to the tibia (Figure 3.9).

Since the bone meshes consisted of Lagrangian elements, they showed non-smooth areas. Cartilage mesh was present at bone mesh areas where cartilage was not present in the segmentations and vice versa. To represent the menisci, three springs per meniscus were used. This seemed to work fine in 0 degrees flexion but seemed unrealistic in 90 degrees of knee flexion because the springs were at an unrealistic angle. A large number of ligaments was included in the model. However, the ligament origins and insertions were embedded in the statistical shape model and were therefore not subject-specific. Next to that, the springs representing the ligaments penetrated the bones. The model was assembled in full extension which was different to the imaging state and therefore the position of the structures could be non-physiological. The moment applied to simulate knee flexion was applied as a rigid body moment on the tibia, which did not coincide with the flexion-extension axis. The stability of the model, the convergence, was highly dependent on small changes in the load-displacement curves of the ligament and mensicus springs.

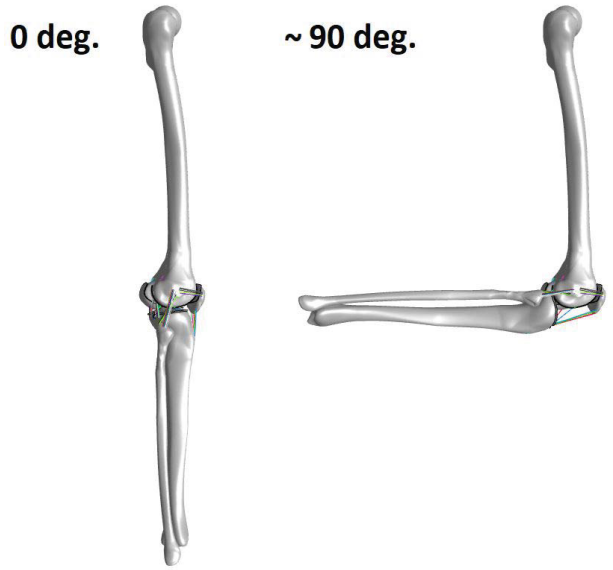

Figure 3.8: Model version 1 in 0 and ~ 90 degrees of knee flexion, lateral view.

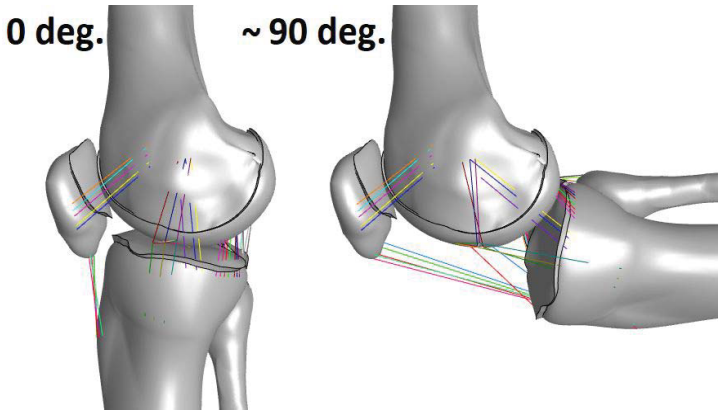

Figure 3.9: Model version 1 in 0 and ~90 degrees of knee flexion, medial view.

3.3.3.2 Model version 2

Compared to model version 1, in model version 2 (Figure 3.10), the model stability increased after changing the ligaments into continuum instead of spring representations and changing the

cartilage-cartilage contact formulations into sliding-elastic contacts. However, the models showed convergence issues in the simulations from 0 to 90 degrees of knee flexion, where both model simulations crashed around 80 degrees of knee flexion.
The oks003 specimen is a left knee dataset, but was modelled as a right knee since the cartilage mesh generation workflow was only functional for right knee joints. The same bone and cartilage mesh generation workflows as in model version 1 were used, which caused the subchondral bone area, and therewith the cartilage mesh, to not be accurate to the segmentations. The oks003 and du02 models shared the same meshed geometries for the ligaments and menisci, which were not specimen-specific for model oks003 and they were put in the model manually. The model was assembled in full extension which was different to the imaging state and therefore the position of the structures could be non-physiological.

Only the four main ligaments were included in this version of the model. There was no penetration of the ligaments into the bones since this was prevented by a ligament-bone contact formulation. All ligaments had the same material model, where only the ligament prestretch factor was optimised to laxity data from the literature. This was only done with the knee in full extension in the direction of anterior-posterior translation and for internal-external rotation. The embedded rigid cylindrical joints enabled the prescription of flexion-extension rotation and the loads to be prescribed on the corresponding anatomical joint axes.

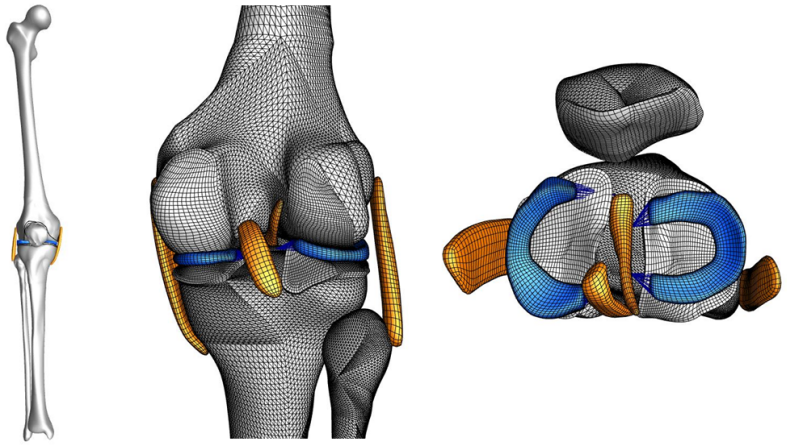

Figure 3.10: Model version 2, anterior view (left), posterior view (middle) and superior view (right).

3.3.3.3 Model version 3

Model version 3 of both datasets was developed successfully (Figure 3.11 & 3.12). After model calibration, as described in Chapter 6, the simulation of 0 to 90 degrees of knee flexion converged fully for model du02. For model oks003, the model converged further compared to version 2 of the model (up to ~84.5 degrees of knee flexion). Before calibration, cartilage-cartilage penetration was present on the medial side of the joint in the 0 to 90 degrees of knee flexion simulation.

In this version of the model, specimen du02 was modelled as a right and specimen oks003 as a left knee. Specimen specific 3D bone, cartilage, ligament and menisci meshes were obtained. The model

was assembled with all geometries in their imaging morphology and position. The cartilages were modelled as rigid bodies and all ligaments had ligament specific material models from the literature. The ligaments were calibrated to specimen-specific data in multiple flexion angles (Chapter 6). The rigid cylindrical joints enabled application of loads and prescribed degrees of freedom in the anatomical coordinate system.

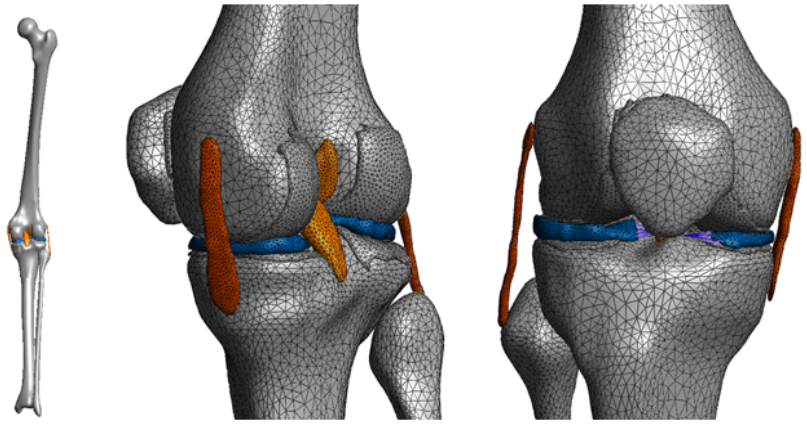

Figure 3.11: Model version 3, du02 dataset. Posterior view (left), medial posterior view (middle) and anterior view (right).

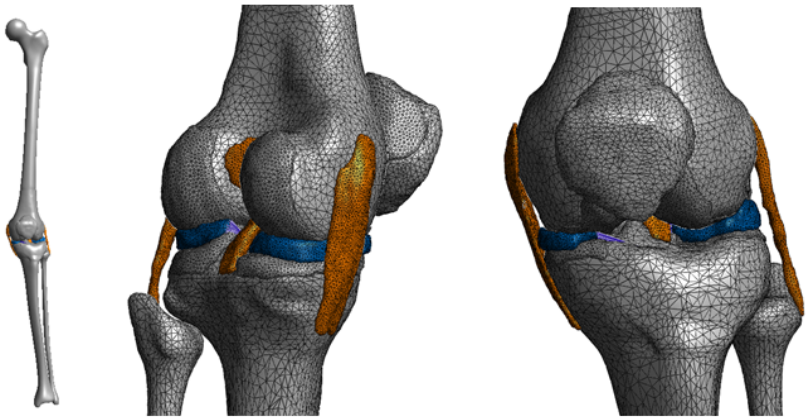

Figure 3.12: Model version 3, oks003 dataset. Anterior view (left), medial posterior view (middle) and anterior view (right).

3.3.4 Discussion & conclusion

Three versions of tibiofemoral knee joint models were developed. Each model improved based on the limitations of the previous model. The results showed that the development of computational knee joint models is an iterative process where many decisions have to be made. Changes to the models were often applied to improve convergence and improve the mechanics to resemble anatomical behaviour. Decisions in model development are a constant trade-off between modelling time, simulation accuracy and convergence time. All these decisions depend on the modeller, and there are multiple right decisions. This results in questionable model reproducibility. A generic model development workflow or a model benchmarking dataset could help increase model reproducibility. This is currently being worked on in the KneeHub project.

3.3.4.1 Model version 1

The goal of the model was to simulate 0 to 90 degrees of knee flexion, which model version 1 did. However, by visually inspecting the passive knee flexion movement, an unrealistic point of rotation was observed, where the femur was located too far posterior relative to the tibia (Figures 3.8 & 3.9). Manually adjusting the ligament properties to obtain a more anatomically correct point of rotation was tried but without success. It is expected that the model might have been underconstrained by not having enough springs representing the ligaments. Also, the springs might not have been implemented well since they penetrated the bones. To obtain a more stable joint, the addition of ligaments and the addition of springs per ligament bundle was investigated. However, this did not solve the problem.

Several limitations of model version 1 were identified. Firstly, all the springs in one ligament bundle had the same optimised stiffness and reference strain. Separately optimising each spring could have given a more stable model. However, this would have increased optimisation time. Secondly, The stability of the model was highly dependent on the menisci load-displacement curves obtained in the optimisation, which is not anatomically correct since the primary function of the menisci is to ensure a better articulation and transferring load. Using continuum elements for the menisci replacing the menisci springs could solve this problem. Thirdly, the SSM used to obtain the bone meshes is based on a Lagrangian mesh, which induces non-smooth areas where the separate Lagrangian elements come together. Then lastly, the cartilage lofting workflow, based on the Lagrangian mesh, does not allow for left knees and is not subject-specific. The areas on the bone where cartilage was lofted from are embedded in the SSM using material points. Because of this, areas on the bone where cartilage should have been present according to the segmentation did not show any cartilage and vice versa.

3.3.4.2 Model version 2

Model version 2 included continuum representations of the ligaments and the menisci. The use of continuum representations of the ligaments provided the ability to avoid penetration by applying a contact between the ligaments and the other structures in the model. This increased the anatomical accuracy of the wrapping behaviour of the ligaments compared to model version 1.

In model version 2, the same ligament and menisci meshes were used for model du02 and oks003. For model oks003, these meshes were not subject-specific. Next to that, the ligaments and menisci were manually put in place, which is dependent on the modeller. This could significantly influence the model outcomes since variations in ligament mesh geometry and attachment sites directly influence the line of action of the ligaments.

The method to obtain the bone and cartilage meshes was kept the same between model versions 1 and 2, with the cartilage mesh generation workflow not being subject-specific and only working for right knees. Therefore dataset oks003 was modelled as a right knee instead of a left knee by mirroring

the segmentation data. This is undesirable because it complicates the interpretation of model outcomes.

The model was only optimised at 0 degrees of knee flexion and not at 0 and 90 degrees as intended. Therefore the load-displacement behaviour in other flexion angles than full extension is most likely incorrect. Next to that, the models were calibrated to literature data instead of subject-specific data.

3.3.4.3 Model version 3

In model version 3, most limitations of models version 1 and 2 were solved. In the 0 to 90 degrees knee flexion simulation, cartilage-cartilage penetration was found on the medial side of the joint. To reduce this penetration, the calibrations (described in Chapter 6) were started with the penalty factor of the cartilage-cartilage contact set to 1 and 10 to investigate if the higher penalty factor decreased penetration.

A couple of limitations to model version 3 should be addressed. Model version 3 did not include the patellofemoral joint, but for future addition, the geometry of the patella bone and cartilage was included without interactions with the other structures. The tibiofemoral cartilages were modelled as rigid bodies, this should be changed to a deformable material model if the cartilage tissue stresses and strains are of interest. The material models of the ligaments used Young's moduli from the literature and were not calibrated. Similarly, the mensici material models were adapted from the literature and were therefore not specimen-specific.

All meshes, except for part of the bone meshes, were manually generated. Ideally, these steps would be automised to decrease mesh generation time and to decrease human interaction. Also, the contacts have to be manually put in by the modeller. For example, the nodes involved in the rigid tied joints between the bones and ligaments. In these manual processes, decisions have to be made which are dependent on the modeller, potentially influencing the model and therewith the model outcomes.

3.3.4 Conclusion

Model development is a creative and challenging process where a lot of decisions have to be made. Changes to the initial modelling plans are common. This was evident in the multiple versions of the model built, where adjustments to the model were made based on the limitations of previous model versions.

References

Ali, A. A., Shalhoub, S. S., Cyr, A. J., Fitzpatrick, C. K., Maletsky, L. P., Rullkoetter, P. J., & Shelburne, K. B. (2016). Validation of predicted patellofemoral mechanics in a finite element model of the healthy and cruciate-deficient knee. *Journal of Biomechanics., 49*(2), 302-309.

Baker, M. (2016). Is there a reproducibility crisis? A Nature survey lifts the lid on how researchers view the crisis rocking science and what they think will help. *Nature, 533*(7604), 452-455.

Bennetts, C. J., Chokhandre, S., Donnola, S. B., Flask, C. A., Bonner, T. F., Colbrunn, R. W., & Erdemir, A. (2015). Open Knee(s): magnetic resonance imaging for specimen-specific next generation knee models. *SB3C2015, Summer Biomechanics, Bioengineering and Biotransport Conference, Utah, USA, June 17-20, 2015.*

Bonner, T. F., Colbrunn, R. W., Chokhandre, S., Bennetts, C., & Erdemir, A. (2015). Open Knee(s): comprehensive tibiofemoral joint testing for specimen-specific next generation knee models. *SB3C2015, Summer Biomechanics, Bioengineering and Biotransport Conference, Utah, USA, June 17-20, 2015*.

Colbrunn, R. W., Bonner, T. F., Chokhandre, S. K., Bennetts, C. J., Halloran J., & Erdemir, A. (2015). Open Knee(s): comprehensive patellofemoral joint testing for specimen-specific next generation knee models. *ASB 2015, 39th Annual Meeting of the American Society of Biomechanics, Columbus, Ohio, USA, August 5-8, 2015*.

Erdemir, A., Bennetts, C., Bonner, T., Chokhandre, S. K., & Colbrunn, R. W. (2015). Open Knee(s): founding data for next generation knee models. *BMES/FDA, Frontiers in Medical Devices Conference: Innovations in Modeling and Simulation, Washington, DC, USA, May 18-20, 2015*.

Erdemir, A., Besier, T. F., Halloran, J. P., Imhauser, C. W., Laz, P. J., Morrison, T. M., & Shelburne, K. B. (2019). Deciphering the “art” in modeling and simulation of the knee joint: overall strategy. *Journal of biomechanical engineering, 141*(7), 071002.

Erdemir, A., & Sibole, S. (2010). Open knee: a three-dimensional finite element representation of the knee joint. User's guide, *version 1*(0).

Grood, E. S., & Suntay, W. J. (1983). A joint coordinate system for the clinical description of three-dimensional motions: application to the knee. *Journal of biomechanical engineering, 105*(2), 136-144.

Harris, M. D., Cyr, A. J., Ali, A. A., Fitzpatrick, C. K., Rullkoetter, P. J., Maletsky, L. P., & Shelburne, K. B. (2016) A Combined Experimental and Computational Approach to Subject-Specific Analysis of Knee Joint Laxity. *Journal of biomechanical engineering, 138*(8), 0810041–0810048.

Kazemi, M. (2018). A Framework to Fuse Subject-Specific Musculoskeletal Models into Knee Finite Element Analyses. *The University of Auckland. ResearchSpace@Auckland*.

Li, G., Gil, J., Kanamori, A., & Woo, S. Y. (1999). A validated three-dimensional computational model of a human knee joint. *Journal of biomechanical engineering, 121*(6), 657-662.

Li, G., Suggs, J., & Gill, T. (2002). The effect of anterior cruciate ligament injury on knee joint function under a simulated muscle load: a three-dimensional computational simulation. *Annals of biomedical engineering, 30*(5), 713-720.

Maas, S.A., Ellis, B.J., Ateshian, G.A., Weiss, J.A. (2012). FEBio: Finite Elements for Biomechanics. *Journal of Biomechanical Engineering, 134*(1), 011005.

Orozco, G. A., Tanska, P., Mononen, M. E., Halonen, K. S., & Korhonen, R. K. (2018). The effect of constitutive representations and structural constituents of ligaments on knee joint mechanics. *Scientific reports, 8*(1), 1-15.

Roth, J. D., Howell, S. M., & Hull, M. L. (2015). Native knee laxities at 0, 45, and 90 of flexion and their relationship to the goal of the gap-balancing alignment method of total knee arthroplasty. *The Journal of Bone & Joint Surgery, 97*(20), 1678-1684.

Zhang, J., Fernandez, J., Hislop-Jambrich, J., & Besier, T. F. (2016). Lower limb estimation from sparse landmarks using an articulated shape model. *Journal of biomechanics, 49*(16), 3875-3881.

Zhang, J., Hislop-Jambrich, J., & Besier, T. F. (2016). Predictive statistical models of baseline variations in 3-D femoral cortex morphology. *Medical engineering & physics, 38*(5), 450-457.

Zhang, J., Sorby, H., Clement, J., Thomas, C. D. L., Hunter, P., Nielsen, P., Lloyd, D., Taylor, M. & Besier, T. (2014). The MAP client: user-friendly musculoskeletal modelling workflows. *International Symposium on Biomedical Simulation*, 182-192.